AlAs-monolayer dependence of the Γ-X coupling in GaAs-AlAs type-II heterostructures

C. Gourdon, D. Martins, and P. Lavallard
Groupe de Physique des Solides, Universités Paris 6 et 7, CNRS UMR 75-88, Tour 23, 2 Place Jussieu, 75251 Paris, Cedex 05, France

E. L. Ivchenko
A. F. Ioffe Physico-Technical Institute, Russian Academy of Sciences, 194021 St. Petersburg, Russia

Yun-Lin Zheng
Laboratoire de Minéralogie-Cristallographie, Universités Paris 6 et 7, CNRS UMR 75-90, 4 Place Jussieu, 75252 Paris, Cedex 05, France

R. Planel*
Laboratoire de Microstructures et Microélectronique (L2M), CNRS UPR 20, 196 Avenue Henri Ravera, 92220 Bagneux, France
(Received 24 May 2000)

For ideal type-II GaAs/AlAs superlattices it was predicted that the coupling between Γ and X_z electron states is allowed (forbidden) if the number of monolayers in AlAs slabs is even (odd). We use a simpler structure, namely, a single GaAs/AlAs/GaAs type-II double quantum well with thickness gradient to show experimental evidence of the AlAs-monolayer dependence of the Γ-X coupling. A careful determination of layer thicknesses is obtained from electron microscopy and optical spectroscopy using additional quantum wells inserted in the structure. The results concerning the Γ-X coupling are obtained from the study of the ratio of photoluminescence intensities of the zero-phonon line and the phonon replica and from their time decay. The variation of the Γ-X coupling with AlAs thickness cannot be explained simply by the variation of the overlap of Γ and X_z envelope functions. It clearly shows the monolayer dependence of the Γ-X mixing potential. We develop a simple model to obtain the Γ-X coupling in the case of nonabrupt interfaces. The amplitude of variation of the radiative recombination time due to the Γ-X mixing is well reproduced within this model.

I. INTRODUCTION

Type-II GaAs/AlAs heterostructures have been the subject of a number of experimental papers in the past years.[1–7] Such topics as the transition from type-I to type-II superlattices[1–3] (SL's) the nature of the lowest electronic states[4–7] (X_z or X_{xy}), and the valley-mixing effects[2,7] (Γ-X coupling) in type-II SL's have attracted considerable attention. Optical studies of type-II SL's have led to good knowledge of their electronic subband structure, opening the way for detailed investigations of the fine structure of exciton states[8,9] and high excitation effects.[10,11] In addition, the study of transport properties in heterostructures has shown that the Γ-X transfer plays a key role.[12,13]

Let us briefly recall the main characteristics of the band structure of GaAs/AlAs SL's.[4] Below a GaAs thickness of 36 Å and provided that the AlAs thickness is not too small, the SL is of type II. The electron and hole wave functions are mostly confined in AlAs and GaAs layers, respectively. The electron wave function is derived from an X state of AlAs. The degeneracy of the X state is lifted by the confinement because of the effective mass anisotropy of the X valley. Owing to the competition between confinement and strain effects, the lowest electron state is an X_z state for AlAs thickness below 70 Å and GaAs thickness above 7–8 Å and an X_{xy} state otherwise (z denotes the [001] growth axis). SL's with X_z as the lowest electron state are usually denoted as pseudodirect since the X_z state is coupled to the Γ state in GaAs. The fundamental optical transition involving the first heavy-hole state (HH_1) and the first X_z-electron state is thus weakly allowed. Photoluminescence (PL) from pseudodirect SL's consists of a prominent zero-phonon (ZPH) line and phonon (PH) replicas. SL's with X_{xy} as the lowest electron state are denoted as indirect.

From the theoretical point of view, the subband structure of type-II $(GaAs)_N/(AlAs)_M$ SL's with $N(M)$ monolayers (ML's) of GaAs(AlAs) in a period was investigated by several authors using a tight binding method,[14,15] an empirical pseudopotential approach,[16–18] or the effective mass approximation with extended boundary conditions;[19–21] see also the latest publications[22–25] on intervalley mixings. The coupling between the lowest Γ and X_z electron states was shown to depend on the parity of the number M of ML's in AlAs slabs. This coupling exists if M is even and cancels if M is odd. Such an effect is seldom encountered in solid-state physics. Yet a similar behavior, although of different origin, was demonstrated in thin metallic layers. The coupling between two ferromagnetic layers separated by a spacer layer was studied for the system Fe/Cr/Fe with a wedged Cr layer. It oscillates between ferromagnetic and antiferromagnetic behavior with increasing Cr thickness, the smallest period being equal to 2.1 ML.[26]

Next we recall the origin of the parity-dependent Γ-X coupling in GaAs/AlAs heterostructures. The Γ and X states are coupled if they are both even under the symmetry operations changing z into $-z$. In the bulk the origin for symme-

try operations is usually taken on an As site.[27] In a SL the origin must be taken at the middle plane of an AlAs or a GaAs slab. The Γ Bloch function as well as the Γ envelope function is even under a symmetry operation that changes z into $-z$ whatever the nature of the plane of origin. The envelope function of the lowest X state is even. If the plane of origin is an As plane in AlAs (even M), the X Bloch function is even and Γ and X states are then coupled. If the plane of origin is an Al plane (odd M), the X Bloch function is odd and Γ and X states are not coupled. This conclusion holds even if the complexity of the real band structure at the X point is taken into account (the existence of X_1 and X_3 states coupled by the $\mathbf{k}\cdot\mathbf{p}$ interaction).[20] In GaAs/AlAs SL's an additional condition must be fulfilled for Γ-X coupling: the bulk zone-edge X point along the [001] direction must be folded onto the zone center Γ point of the SL Brillouin zone. This is achieved if $(N+M)$ is even or, in other words, if the SL period $P=(N+M)a_0/2$ is an even number of ML's of thickness $a_0/2$. It stems from the fact that alternate (001) planes of the same element do not lie on top of each other.

There have been several attempts to demonstrate experimentally the parity effect in SL's. For $(\mathrm{GaAs})_M/(\mathrm{AlAs})_M$ SL's with $8\leqslant M\leqslant 15$ it was observed that the radiative recombination rate is larger for odd M.[28] This result, which is opposite to the predicted one, was not explained. However, a similar study for SL's of the same composition did not show any dependence of the radiative recombination rate on the parity of M (Ref. 29) and neither did a comprehensive study of PL from short-period SL's in Ref. 7. Some hints of the parity effect could nevertheless be inferred from time-resolved PL studies of SL's.[30] The nonexponential decay of the PL from type-II pseudodirect SL's was attributed to the existence of a distribution of the values of the radiative probability $w_{\Gamma X}$ due to the Γ-X coupling. Excitons that contribute to the PL line are localized in regions with slightly different AlAs effective layer thicknesses. Therefore $w_{\Gamma X}$ varies from site to site because of the parity effect. Layer thickness fluctuations make the parity effect difficult to demonstrate experimentally. In the case of a SL, fluctuations of the layer thickness exist not only in the layer plane but also along the growth axis. The possibility of the occurrence of a slightly enlarged well for electrons among the AlAs layers can never be ruled out.

We have undertaken a study of the optical properties of GaAs/AlAs type II structures with the aim of revealing the ML dependence of the Γ-X coupling. Considering the necessity to control as much as possible the quality of interfaces, e.g., by using growth interruptions, the use of a single GaAs/AlAs/GaAs double quantum well (DQW) of type II is more appropriate. It can be shown that the Γ-X coupling depends on the parity of M in the same manner as for a GaAs/AlAs SL.[31] Besides, despite the good reproducibility of growth conditions from one sample to the next in the molecular beam epitaxy (MBE) growth chamber, it is preferable to grow on the same sample different regions with an even and an odd number of AlAs ML's or, in other words, a sample with a gradient of AlAs-layer thickness. This paper is organized as follows. In Sec. II we discuss the limitations for the composition of a DQW appropriate to the study of the parity effect. Then we describe the samples and the experimental techniques used to characterize and study them. In Sec. III we present the procedure used to determine the GaAs- and AlAs-layer thicknesses. Section IV is devoted to an analysis of the experimental results. We show the experimental and calculated transition energies and present the results on the dependence of the Γ-X coupling matrix element on the AlAs thickness. We develop in Sec. V a simple model of Γ-X coupling taking into account interface roughness. Section VI is devoted to a discussion of the experimental results in the frame of this model. Finally we summarize our results and conclude in Sec. VII.

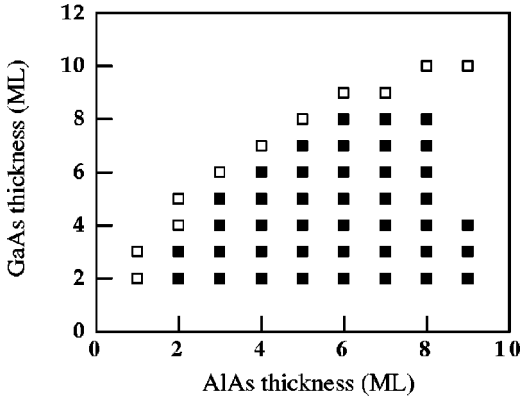

FIG. 1. Map of the GaAs and AlAs thicknesses in a GaAs/AlAs/GaAs type-II DQW of appropriate composition to observe the ML dependence of the Γ-X coupling (solid squares). The open squares represent type-I DQW's.

II. SAMPLE COMPOSITION AND EXPERIMENTAL TECHNIQUES

A. Composition of the DQW

In order to be suitable for the study of the AlAs-monolayer dependence of the Γ-X coupling the composition of the DQW must fulfill a few requirements. The DQW must be embedded in a $\mathrm{Ga}_{1-\xi}\mathrm{Al}_\xi\mathrm{As}$ alloy with concentration ξ such that the X_z and the Γ electron states are indeed confined in the double well. The GaAs layers must be thin enough to ensure that the Γ state is at higher energy than the X_z state. The maximum thickness of the AlAs layer is fixed by the following condition: the difference ΔE_h of the energies of the hole states with symmetrical and antisymmetrical envelope functions must be larger than the thermal energy k_BT. In the case of odd M, the lowest electron state is an antisymmetrical X_z state which is coupled to an antisymmetrical Γ state. If the condition on ΔE_h is not fulfilled, electrons can recombine with holes in the thermally populated antisymmetrical hole state, leading to the observation of the opposite parity selection rule. From the above conditions we determine the domain of GaAs- and AlAs-layer thicknesses suitable to observe the parity effect. Figure 1 shows this domain for a $(\mathrm{GaAs})_N/(\mathrm{AlAs})_M$ DQW in a $\mathrm{Ga}_{0.55}\mathrm{Al}_{0.45}\mathrm{As}$ alloy at a temperature of 2 K. Typically the number of ML's, N or M, lies between 2 and 8.

B. Samples and experimental techniques

The samples are grown by MBE. A large gradient of AlAs thickness across the wafer is achieved by stopping the rotation of the substrate during the growth of AlAs. The composition of wafer A is the following. On top of the

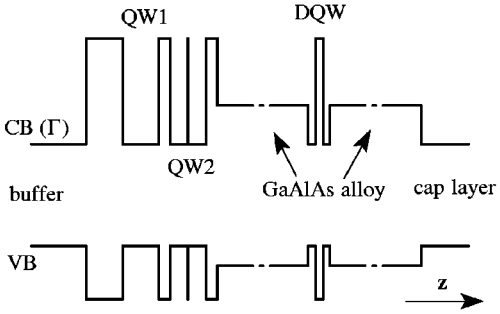

FIG. 2. Schematic representation of the band structure [Γ conduction band (CB) and valence band (VB)] of the samples used in this work (not to scale).

n^+-Si-doped GaAs buffer we first grew a number of layers that are used for optical calibration of GaAs and AlAs thicknesses. This calibration structure consists of two 100-Å GaAs quantum wells (QW's) separated by a 30-Å AlAs barrier. In the middle of the second GaAs QW (QW2), 1 ML of AlAs was deposited while the rotation of the substrate was stopped. Growth interruptions of 120 s were achieved before and after the AlAs-ML growth. Then the main structure for the study of the parity effect was grown. It consists of a DQW of nominal composition at the center of the wafer GaAs(6 ML)/AlAs(6 ML)/GaAs(6 ML) sandwiched between two $Ga_{0.6}Al_{0.4}As$ layers of thickness 1000 Å. The AlAs layer is grown in the same conditions as in the calibration structure. The band structure is schematically shown in Fig. 2. The 500-Å GaAs cap layer is n^+ doped as the buffer layer in order to pin the Fermi level at the bottom of the GaAs conduction band in the whole structure and to avoid built-in electric fields and band curvature. GaAs is grown at a substrate temperature of 600 °C. AlAs in QW2 and in the DQW is grown at 640 °C (the temperature is raised from 600 to 640°C during the 120-s growth interruption). Sample A1 (3×50 mm^2) was cleaved along the diameter of the wafer in the [110] direction. PL is studied as a function of the position of the laser spot on the sample. Smaller pieces, sample A2 and sample A3, were cleaved near the center and the edge of wafer A, respectively, close to sample A1. They were first characterized by optical spectroscopy and then by transmission electron microscopy (TEM).

The composition of wafer B is close to that of wafer A. Wafer B contains a calibration structure and a DQW. The buffer and cap layer are not doped. The nominal composition of the DQW structure at the center of the wafer is GaAs(4 ML)/AlAs(4 ML)/GaAs(4 ML) for the DQW and $Ga_{0.55}Al_{0.45}As$ (992 Å) for the alloy cladding. Additional growth interruptions of 120 s are achieved before the first GaAs QW and after the second one in the DQW structure. Unfortunately the rotation of the substrate was not stopped during the growth of the AlAs ML in QW2. Therefore the gradient of AlAs determined in the calibration structure may be somewhat different from the one in the DQW. Samples B1 and B2 were cleaved from wafer B along the $[1\bar{1}0]$ and the [110] radius, respectively. Samples B3 and B4 were cleaved near the center and the edge of the wafer respectively, close to sample B1. They were used for TEM measurements.

Wafer C was made similar to wafer A with some improvements. The last 100 Å of the buffer layer were not doped in order to prevent segregation of the dopants into the calibration structure. The growth temperature was kept at 600 °C for GaAs as well as for AlAs in order to prevent Ga evaporation during the growth interruptions. Sample C1 (4×50 mm^2) was cleaved along the diameter of the wafer in the [110] direction. No TEM measurements were made for this wafer. Attempts to obtain a larger AlAs thickness gradient by tilting the substrate holder were not successful. Poorer sample quality was obtained, as indicated by the broadening of the PL lines.

Sample D was used for thickness calibration by x-ray diffraction. It consist of a calibration structure followed by a SL of nominal composition GaAs(6 ML)/AlAs(8 ML) grown in the same conditions of growth temperature and growth interruptions as wafer A. For this sample the rotation of the substrate was not stopped during the growth of AlAs.

Samples were prepared for TEM measurements first using a mechanical thinning and then an Ar^+ ion milling. The TEM study were performed using 200-kV JEOL 2000EX, Topcon EM002B and Philips CM20 electron microscopes. Both conventional and high-resolution observations were made on the cross-section setting. Conventional imaging, namely the dark field imaging with 002* spot, allows one to get a good chemical contrast between GaAs and AlAs. The AlAs ML in QW2 of the calibration structure can be easily revealed. With high-resolution lattice images, layer thicknesses of the calibration structure were precisely determined.

PL was excited with the 514-nm line of an argon ion laser. Care was taken to use very low excitation power density (typically less than 50 mW cm^{-2}) to avoid the broadening and shift of the main PL line to higher energy. For time-resolved PL, laser pulses were generated with a 250-MHz acousto-optical modulator. 50-ns pulses with a 50-μs period and an extinction ratio better than 1:1000 were used. PL was focused onto a monochromator slit and detected with a time-correlated single photon counting system. For photoluminescence excitation (PLE) spectra of the calibration structure we used a continuous-wave Ti-sapphire laser pumped by an argon laser with a light regulation system. For PLE spectra of the DQW a rhodamine 6G-dye laser was used.

III. CALIBRATION OF GaAs AND AlAs THICKNESSES

A. X-ray diffraction

Results from x-ray diffraction for sample D containing a SL show that the thickness of GaAs layers in the SL is smaller than the nominal one by 1.4 ML whereas the AlAs thickness is very close to the nominal one. This is the result of the evaporation of Ga atoms during the growth interruption and the concomitant raise of the substrate temperature from 600 to 640 °C after completion of each GaAs layer. This interpretation is confirmed by direct measurement of Ga evaporation rate (0.05 Å s^{-1}) exactly in the same growth conditions. As a consequence both QW2 and the DQW are asymmetrical in samples A1, B1, and B2, the first GaAs layer being thinner than the second one by 1.4 ML. This is taken into account in the calculation of transition energies in

the following. The asymmetry of the structure has proved to be quite essential for the interpretation of PL spectra from samples B1 and B2.

B. Determination of layer thickness by optical spectroscopy and TEM

The photon energies of the PL lines from QW1 (nominally 100 Å GaAs in the center of the wafer) and QW2 (nominally 100 Å GaAs with 1 ML of AlAs in the middle) are used to obtain the gradient of GaAs and AlAs thickness. The PL spectra of QW1 and QW2 was recorded each 2 mm along the samples. PLE spectra were recorded at a few positions to determine the value of the Stokes shift between absorption and PL. From the energy of the lowest Γ_1-HH_1 excitonic transition in QW1 we determine the GaAs thickness in QW1. From the difference Δ_{12} of the Γ_1-HH_1 transition energies in QW1 and in QW2, we determine the amount of AlAs in the middle of QW2. Δ_{12}, which is of the order of 50–60 meV, is extremely sensitive to the thickness of AlAs. Its variation is about 1 meV for 0.1 Å.

The relation between the thickness L and the transition energy E in QW1 is obtained as follows. We calculate the intersubband Γ_1-HH_1 transition energy as a function of L in the effective-mass approximation using abrupt interfaces and taking into account the nonparabolicity of the conduction band.[32] The exciton binding energy as a function of the well thickness is taken from Ref. 33. Combining these results and interpolating between the calculated values we obtain the following relation:

$$E_{meV}(L_{\text{Å}}) = \sum_{i=0}^{5} q_i L^i \tag{3.1}$$

with $q_0 = 2.296\,30$, $q_1 = -28.2650$, $q_2 = 4.785\,44 \times 10^{-1}$, $q_3 = -4.388\,13 \times 10^{-3}$, $q_4 = 2.100\,64 \times 10^{-5}$, and $q_5 = -4.119\,72 \times 10^{-8}$. We check the validity of this equation for L around 100 Å by comparing these results with TEM measurements for wafer B. From high-resolution TEM micrographs of sample B3 we determine the average thickness of QW1 to be equal to 86.21 ± 1.36 Å from 30 measurements over an in-plane distance of 600 Å. No optical measurements were done on sample B3 prior to TEM observations. Therefore the value of 86.21 Å has to be compared to the thickness obtained from optical determination for sample B1 closest to sample B3, i.e., at positions 28 mm or 30 mm. Our calculation gives 85.39 Å and 84.16 Å for these points, respectively. It is in very good agreement with TEM results. More precisely we can say that the calculated thickness is at most overestimated by 0.55 Å or underestimated by 3.41 Å. A calculation of the Γ_1-HH_1 transition energy using nonabrupt interfaces leads to even better agreement. The GaAs growth rate at the center of the wafer, 1.54 Å s^{-1}, is obtained by dividing the thickness by the growth duration. In order to calculate the AlAs thickness in QW2 we use the following procedure. From the GaAs growth rate obtained as above and from the growth duration we determine the thickness of the left and right GaAs parts of QW2. We subtract 1.4 ML from the left part to take into account the evaporation of Ga during the growth interruption and temperature rise. We then adjust the AlAs thickness until the energy difference Δ_{12} is equal to the experimental value. Let us compare the AlAs thickness value obtained by this procedure and the value from TEM measurements nearby the center of wafer B. The growth rate of GaAlAs is obtained from the alloy thickness on TEM micrographs. To obtain the AlAs growth rate we subtract the GaAs growth rate. For sample B3, the average AlAs thickness in QW2 obtained by multiplying the AlAs growth rate by the growth duration is found equal to 0.94 ML. This value has to be compared to the one obtained by optics: 0.92 ML and 0.89 ML for positions 28 and 30 mm on sample B1, respectively. When we calculate transition energies using nonabrupt interfaces and the spreading of the AlAs ML in QW2 over 3 ML, the agreement between the calculated value (0.97 ML and 0.94 ML for positions 28 mm and 30 mm) and the one determined by TEM (0.94 ML) is even better. Using the ratio of growth duration for layers in the calibration structure and in the DQW we finally obtain the GaAs and AlAs layer thicknesses in the DQW for samples B1 and B2 as is shown in Fig. 3. The GaAs thickness is that of the second GaAs well, grown without Ga evaporation.

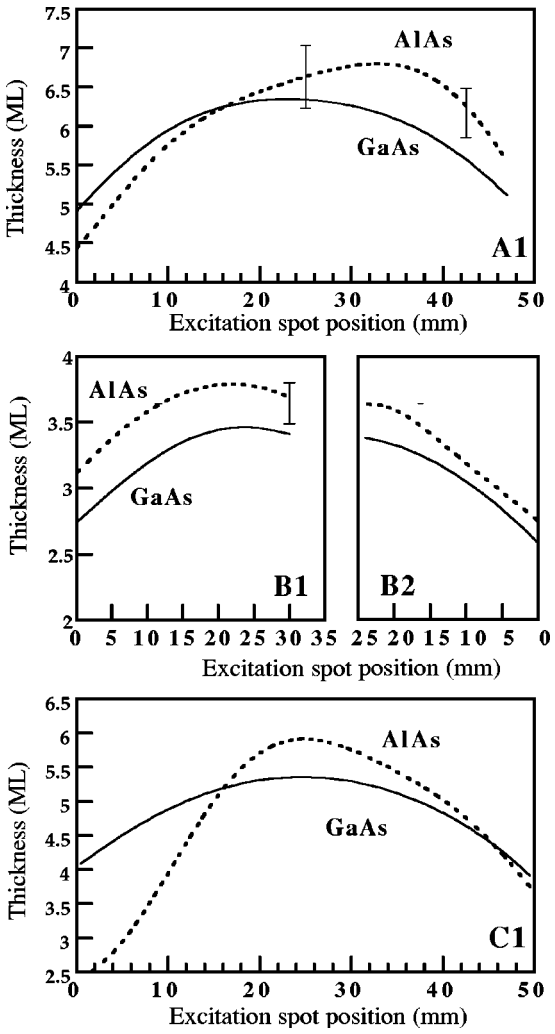

FIG. 3. GaAs and AlAs layer thickness for the DQW in samples A1, B1, B2, and C1.

For sample A we use a different procedure to overcome a few problems related to the doping of the buffer. The PL of QW1 is broad (6–10 meV) and Stokes shifted by 8–10 meV

from the absorption edge observed in PLE spectra. This absorption edge does not show sharp excitonic features but broadbands. On the contrary the PL and PLE spectra of QW2 show the usual excitonic behavior. We conclude that Si dopants have migrated at least into the first AlAs barrier.[34] Their ionization leads to an important density of carriers in QW1 which we evaluate to be 1.3–1.6 10^{11} cm^{-2}. The corresponding Fermi level lies in the Γ_1 subband of QW1 but below the Γ_1 subband of QW2. Therefore the value of GaAs thickness in QW1 is primarily not determined from optics but from high-resolution TEM micrographs. We obtain 105.80 ± 2.77 Å and 93.0 ± 2.38 Å from samples A2 and A3 near the center and the edge of wafer A, respectively. We use these values to calculate the Γ_1-HH_1 transition of the undoped well. The difference δ between the calculated and experimental values is interpolated along sample A1 and the GaAs thickness of QW1 is determined as a function of position along sample A1. The AlAs content of QW2 in samples A2 and A3 is obtained as previously from TEM data. The AlAs gradient along sample A1 is obtained following the procedure described above. Finally, we determine the GaAs and AlAs thicknesses in the DQW. The curves are shown in Fig. 3. Error bars for AlAs thickness are determined from the uncertainty in both the GaAs thickness in QW1 and the alloy thickness obtained from TEM data for samples A2 and A3. For instance, at position 25 mm, the AlAs thickness is found to be equal to 6.65 ± 0.4 ML.

For sample C1 PL and PLE spectra of QW1 and QW2 do not show any indication of dopant migration. Therefore the layer thicknesses are determined from optical data. Figure 3 shows the GaAs and AlAs thicknesses in the DQW. Finally, let us remark that the procedures used either with TEM data (averaging over sample thickness and in-plane distance) or with optical data (use of PLE spectra) lead to a determination of layer thicknesses which are relevant for a free exciton delocalized in the layer plane.

IV. EXPERIMENTAL RESULTS AND ANALYSIS

A. PL spectra

PL spectra of all samples show the usual features of type-II pseudodirect structures: a ZPH line with phonon replicas PH_1, PH_2, or PH_3 at 49 meV, 34.5 meV, and 28 meV, respectively (Fig. 4). PH_2 and PH_3 are not well separated as observed for SL's with thin layers.[35] The PH replicas are attributed to recombination assisted by a zone-edge LO phonon of AlAs (PH_1) and a zone-edge LA phonon of GaAs or AlAs (PH_3). PH_2 may be a superposition of replicas involving zone-edge and zone-center GaAs LO phonons or may originate from a GaAs interface phonon.[35] PL spectra of samples from wafers A and C on the one hand and wafer B on the other hand show a striking difference which is obviously related to the growth process. At any point on samples A1 and C1 one observes a single ZPH line, 6–10 meV broad, originating from the X_z-HH_1 excitonic recombination, together with its PH replicas. The energy of the ZPH line varies smoothly along the sample as shown in Fig. 5. On the contrary, at a few positions on samples B1 and B2, there is an abrupt change of the energy of the ZPH line with coexistence of two lines over a distance of 2–4 mm (Fig. 5). The significant difference in the growth process of wafers A and C and wafer B is the introduction of additional growth interruptions for wafer B at the interfaces GaAlAs/GaAs and GaAs/GaAlAs before and after the growth of the DQW, respectively. Therefore we attribute the ZPH line splitting to the coexistence of large areas of GaAs whose thicknesses differ by 1 ML. The asymmetry of the DQW (the first GaAs well is thinner than the second one on the average) makes it possible to observe PL from excitons localized in sites where the thicknesses of the two GaAs wells either are equal or differ by 1 ML. The X_z-HH_1 transition energies for samples B1 and B2 are shown in Fig. 5. They are calculated in the effective mass and envelope function approximation. The excitonic binding energy and the stress effect in AlAs and in the alloy are not taken into account. The notation $(m/\mathrm{AlAs}/p)$ means that we use a constant GaAs thickness of $m(p)$ ML in the first (second) well and the continuously varying AlAs thickness determined in the previous section. In Fig. 5 the calculated energies have been downshifted by 13 meV. The good agreement between calculated and experimental curves is strong support of the validity of our interpretation. It brings along two comments. First let us note that samples B1 and B2 were in principle excellent candidates to observe the parity effect. In the range of layer thickness (3–4 ML) of these samples, the line splitting due to the variation of AlAs thickness by 1 ML would be of the order of 10 meV. However, despite optimized growth conditions, it was impossible to observe line splittings due to a variation of AlAs thickness by 1 ML. Second, in order to show the parity effect, one needs to study the ratio of the ZPH line and the PH replicas. The existence, at some positions, of two ZPH lines and the overlap of their PH replicas is then a major problem.

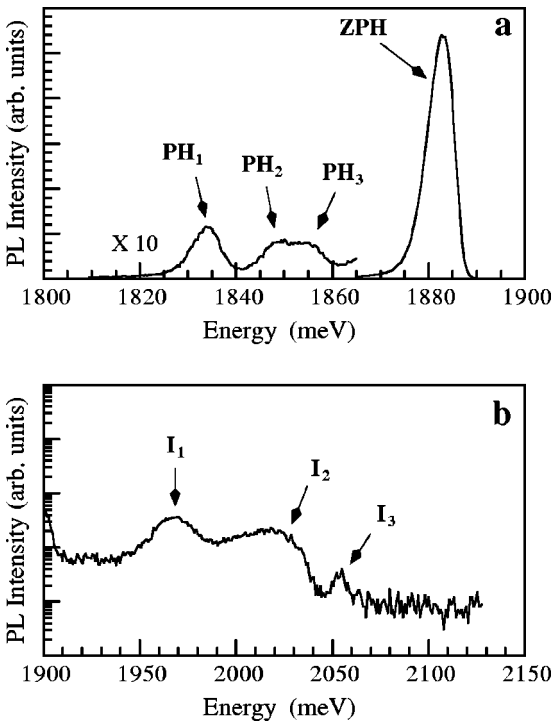

FIG. 4. PL spectrum of sample A1 at position 37 mm. Spectra (a) and (b) are obtained with excitation power densities 50 $mW\,cm^{-2}$ and 50 $W\,cm^{-2}$, respectively. The nature of the PL lines is given in the text.

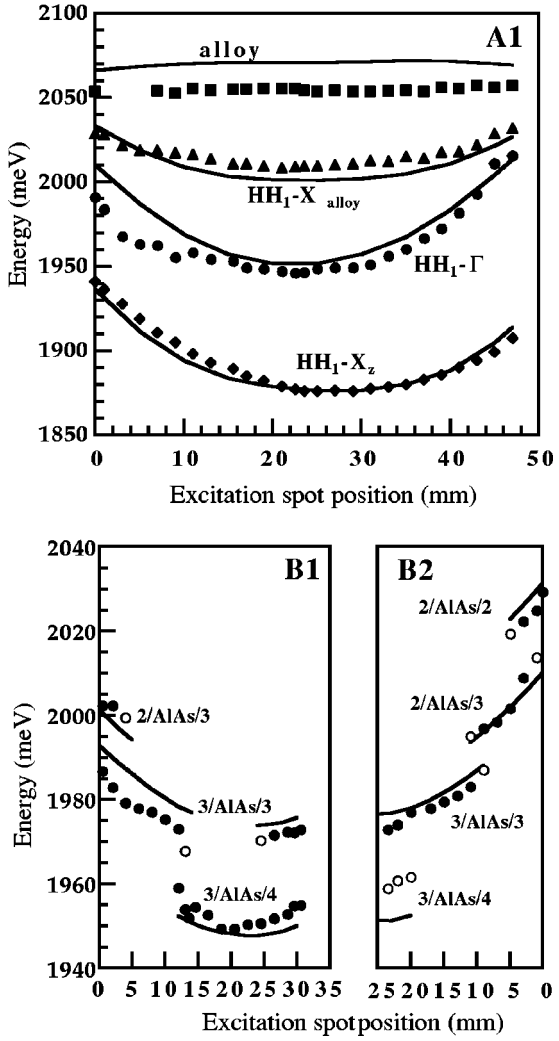

FIG. 5. Transition energies, experimental (circles) and calculated (solid lines), in samples A1, B1, and B2. For samples B1 and B2 solid (open) circles indicate intense (weak) PL intensity.

The study of the Γ-*X* coupling requires the knowledge of the energy difference $(E_\Gamma - E_X)$. It can be obtained from PLE spectra but also more conveniently from PL spectra at moderate excitation density (about 50 W cm^{-2}). However, for samples B1 and B2 we could observe the Γ-HH_1 transition neither in PLE spectra nor in PL spectra. This is in agreement with our calculations: the Γ-HH_1 transition energy lies very close (within a few meV) to the indirect gap of the $Ga_{0.55}Al_{0.45}As$ alloy. For wafers A and C the composition of the alloy was changed to make the Γ-HH_1 transition of the DQW observable. Figure 4 shows the weak lines I_1, I_2, and I_3 observed in PL spectra of sample A1 under moderate excitation power density. In accordance with calculated transition energies (Fig. 5) they are attributed to the Γ-HH_1 transition in the DQW (I_1), to a transition involving the HH_1-hole state in the DQW and the *X* electron in the alloy (I_2) and to the indirect exciton transition in the alloy (I_3). In Fig. 5 the calculated transition energies (except the alloy gap) are upshifted by 26 meV. Calculation of transition energies using nonabrupt interfaces would lead to larger transition energies, more in accordance with the experimental ones.

B. Experimental study of the Γ-*X* coupling

1. Time-integrated PL

In order to determine the dependence of the Γ-*X* coupling matrix element on AlAs thickness we have studied the ratio of the intensities of the ZPH line and the LO_{AlAs} PH replica. In the first approach we consider no dispersion of the radiative recombination rate. The intensity of the ZPH line is proportional to

$$I_{zph} \propto \frac{w_{\Gamma X}}{w_{\Gamma X} + \sum_i w_{ph}^i + w_{nr}}, \tag{4.1}$$

where $w_{\Gamma X}$ is the recombination rate due to the Γ-*X* coupling, w_{ph}^i is the recombination rate due to the phonon-assisted transition with phonon *i*, and w_{nr} is the nonradiative recombination rate. The intensity of the LO PH replica is proportional to

$$I_{ph} \propto \frac{w_{ph}^{LO}}{w_{\Gamma X} + \sum_i w_{ph}^i + w_{nr}}. \tag{4.2}$$

In second-order perturbation theory the recombination rates $w_{\Gamma X}$ and w_{ph}^{LO} are written as

$$w_{\Gamma X} = w_0 \left| \frac{M_{\Gamma X}}{E_\Gamma - E_X} \right|^2, \tag{4.3}$$

$$w_{ph}^{LO} = w_0 \left| \frac{M_{\text{el-ph}}}{E_\Gamma - E_X + h\nu_{ph}} \right|^2, \tag{4.4}$$

where w_0 is the Γ-HH_1 radiative recombination rate for localized excitons,[36] $h\nu_{ph}$ is the LO phonon energy, and $M_{\Gamma X}$ and $M_{\text{el-ph}}$ are the matrix elements of the Γ-*X* coupling and of the electron-phonon interaction connecting Γ and *X* states. It is instructive to present $M_{\text{el-ph}}$ as a product $M^0_{\text{el-ph}} \langle \psi_\Gamma | \psi_X \rangle$, where $M^0_{\text{el-ph}}$ is the matrix element between the Bloch functions and $\langle \psi_\Gamma | \psi_X \rangle$ is the overlap integral which varies along the sample.

Let us note that $M_{\text{el-ph}}$ is independent of the parity of the number *M* of AlAs ML's since the symmetry of the LO phonon state changes with *M* in the same manner as the symmetry of the electron Bloch *X* state.[27] According to Eqs. (4.3) and (4.4) the ratio I_{zph}/I_{ph} is given by

$$\frac{I_{zph}}{I_{ph}} = \left| \frac{M_{\Gamma X}}{M_{\text{el-ph}}} \frac{E_\Gamma - E_X + h\nu_{ph}}{E_\Gamma - E_X} \right|^2. \tag{4.5}$$

In order to demonstrate that the Γ-*X* coupling depends on the parity of *M*, one has to compare the experimental value of I_{zph}/I_{ph} to the ratio $R = (E_\Gamma - E_X + h\nu_{ph})^2/(E_\Gamma - E_X)^2$. Figure 6 shows the experimental ratio of the spectrally integrated intensities I_{zph} and I_{ph} for samples A1 and C1 and the ratio *R* for sample A1. The exponential tail of the ZPH line was subtracted from the PH replica before integrating. The nonmonotonous variation of I_{zph}/I_{ph} is a clear indication of the ML dependence of the Γ-*X* coupling. The ratio I_{zph}/I_{ph} varies by a factor 1.7 in sample A1 and 2.4 in sample C1. The amplitude of variation of I_{zph}/I_{ph} is larger in sample C1

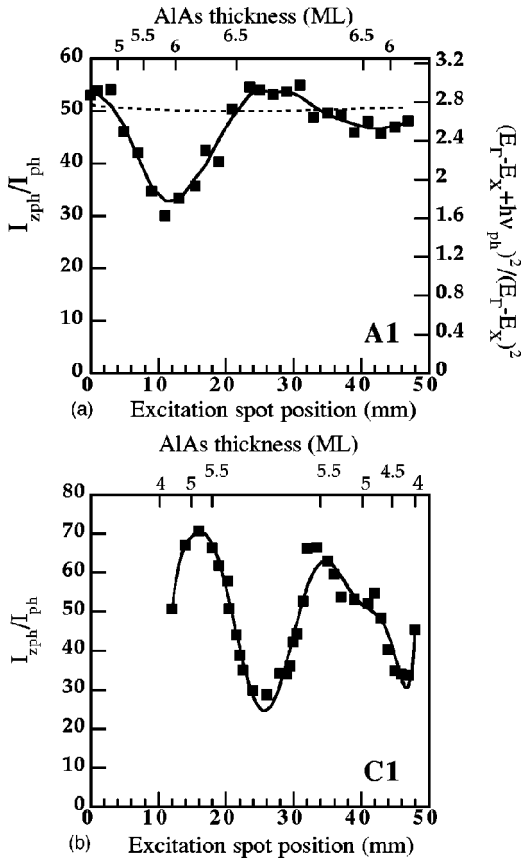

FIG. 6. (a) Experimental ratio I_{zph}/I_{ph} (squares) and ratio $R=(E_\Gamma-E_X+h\nu_{ph})^2/(E_\Gamma-E_X)^2$ (dotted line) as a function of position on sample A1. (b) Experimental ratio I_{zph}/I_{ph} for sample C1. This ratio cannot be obtained between positions 0 and 10 mm. In this region the disappearance of PH replica and the behavior of the ZPH line indicate a type-II to type-I transition. The solid lines are a guide for the eyes.

because the DQW is more symmetrical. The periodic behavior of the Γ-X coupling is also better observed in sample C1.

Figure 7 shows the same data for samples B1 and B2. At positions where two ZPH lines coexist the PL spectrum is decomposed in Gaussian lines. We plot the ratio of intensities of the most intense ZPH line over its LO_{AlAs} PH replica. The ratio I_{zph}/I_{ph} varies in the range 12–40 for sample B1 and 20–75 for sample B2. The values of this ratio close to the center of the wafer [position 30 (25) mm for sample B1 (B2)] are in accordance for the two samples. The theoretical ratio R is obtained from the calculated values of E_Γ and E_X. The discontinuities in the R curve originate from the difference of the E_Γ energies calculated for a $(m/\mathrm{AlAs}/p)$ and a $(m/\mathrm{AlAs}/p+1)$ structure with infinite extension in the layer plane. In fact the Γ-X coupling as well as the electron-phonon coupling occurs via all the Γ states either localized or extended in the layer plane. The discontinuities would be smeared out if the full calculation of $w_{\Gamma X}/w_{ph}$ were performed. R is actually almost constant since the difference $(E_\Gamma-E_X)$ is much larger than the phonon energy. Obviously the amplitude of the variation of I_{zph}/I_{ph} cannot be explained by the variation of R. As we shall see below, for samples B1 and B2 the general behavior of I_{zph}/I_{ph} can be explained by the parity effect with the AlAs gradient determined in Sec. III. The ML line splitting observed in PL

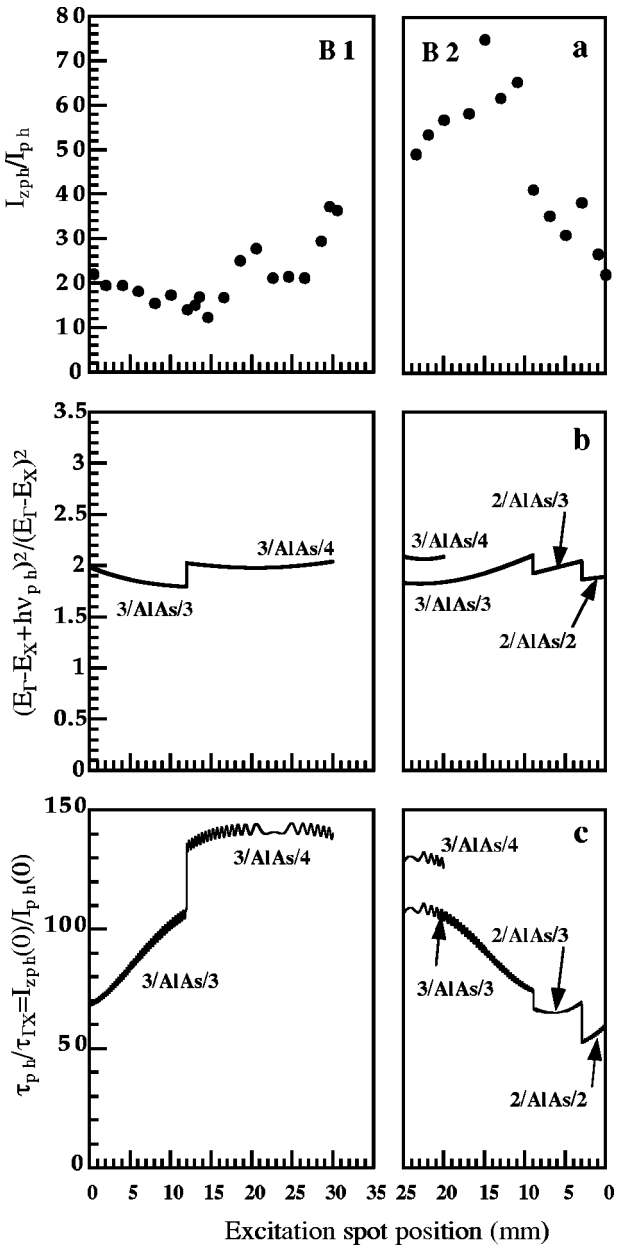

FIG. 7. (a) Experimental ratio I_{zph}/I_{ph}, (b) calculated ratio $R=(E_\Gamma-E_X+h\nu_{ph})^2/(E_\Gamma-E_X)^2$, and (c) calculated ratio $\tau_{ph}/\tau_{\Gamma X}=I_{zph}(0)/I_{ph}(0)$ as a function of position on samples B1 and B2.

spectra shows clearly that exciton localization is governed by the hole localization in large islands of GaAs. The island size is probably much larger than the exciton Bohr radius. The effective AlAs thickness for the localized exciton is indeed the one determined from optical measurements and TEM results.

For samples A1 and C1 the ratio I_{zph}/I_{ph} shows minima at positions where the average AlAs thickness is about 6 ML (A1 and C1) and 4 ML (C1): it seems that the observed parity effect is opposite to the theoretical one. There are two possible explanations. The first one is related to the interface profiles. It was shown theoretically that with quite different GaAs/AlAs and AlAs/GaAs interface profiles, one of them abrupt and the other extending over several ML's, the parity rule for Γ-X coupling is inverted.[18] However, we shall see in detail in Sec. V that, with the interface profiles expected

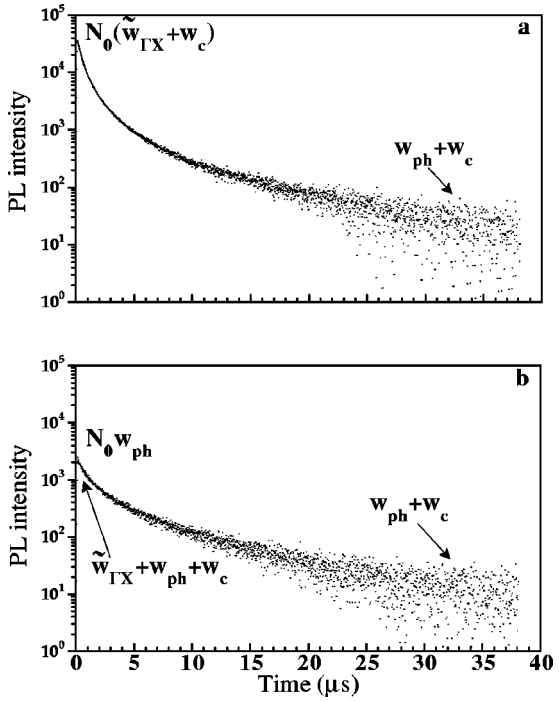

FIG. 8. Decay curves of the ZPH line and the LO PH replica for sample A1 at position 13 mm.

from the growth conditions, there is no inversion of the parity rule. The second explanation is related to exciton localization. A direct proof of exciton localization is unfortunately difficult to obtain since the Stokes shift between absorption and PL cannot be measured in a single type-II DQW because of the very weak absorption coefficient. Considering the nature of the PL spectra, i.e., a single ZPH PL line whose energy shifts smoothly with sample composition, interface roughness is most probably characterized by in-plane small-scale fluctuations of the interface plane of 1 or 2 ML. These fluctuations are averaged over the relative motion of the electron and the hole. The effective localizing potential for the center-of-mass motion of the exciton has minima with larger in-plane length scale. Excitons are very likely localized in regions where the effective AlAs thickness is larger than the average thickness determined above. An effective thickness larger by ~ 1 ML brings our results in accordance with the predicted parity effect.

2. Time-resolved PL

To go one step further one needs to determine separately the recombination rates $w_{\Gamma X}$ and w_{ph}^{LO}. Time-resolved PL experiments were performed for sample A1. The time decay was recorded at the maximum of the ZPH line and at the maximum of the LO phonon replica with the monochromator slits sufficiently open to record most of the PL signal of each line (see Fig. 8). We subtracted in both cases the weak constant PL signal excited by the residual laser signal between laser pulses. We also subtracted from the decay curve of the PH line the decay curve of the tail of PL signal superimposed on the PH line. This decay curve is recorded at about 10 meV below the PH line. In both the ZPH line and the PH replica the decay is nonexponential. Let us note that the spectral shift of the ZPH line obtained from two spectra, one recorded during the first μs after the pulse and the time-integrated one, is very small, less than 0.3 meV. Therefore the spatial and spectral diffusion of excitons can be neglected in the first approach. We attribute the nonexponential decay to the existence of a distribution $p(w_{\Gamma X})$ of the $w_{\Gamma X}$ recombination rates for localized excitons. The time-dependent PL intensities are written as

$$I_{zph}(t)=N_0\int_0^\infty w_{\Gamma X}p(w_{\Gamma X}) \times\exp\left[-\left(w_{\Gamma X}+\sum_i w_{ph}^i+w_{nr}\right)t\right]dw_{\Gamma X}, \tag{4.6}$$

$$I_{ph}(t)=N_0 w_{ph}\int_0^\infty p(w_{\Gamma X}) \times\exp\left[-\left(w_{\Gamma X}+\sum_i w_{ph}^i+w_{nr}\right)t\right]dw_{\Gamma X}, \tag{4.7}$$

where N_0 is the exciton density at $t=0$ and w_{ph} stands for w_{ph}^{LO}. In the following we shall neglect the nonradiative recombination which is very small.[30] The differential decay time in the time window 15–35 μs is about 15 μs. The decay behavior is the same in the ZPH line and the replica at long times ($t>10$ μs). This was also observed for SL's.[37] This time behavior can be well reproduced using a distribution such that $p(w_{\Gamma X})$ is equal to zero for $w_{\Gamma X}$ smaller than a cutoff value w_c of about 15 μs^{-1}. The average value of $w_{\Gamma X}$ is $\langle w_{\Gamma X}\rangle=\int_{w_c}^\infty w_{\Gamma X}p(w_{\Gamma X})dw_{\Gamma X}$. We shall define $\tilde{w}_{\Gamma X}$ as $\tilde{w}_{\Gamma X}=\langle w_{\Gamma X}\rangle-w_c$. The important parameters $\tilde{w}_{\Gamma X}$, w_{ph}, and w_c are obtained from a simple analysis of the decay curves $I_{zph}(t)$ and $I_{ph}(t)$. We use the following experimental data: the ratio of $I_{zph}(t)$ and $I_{ph}(t)$ at $t=0$,

$$\frac{I_{zph}(0)}{I_{ph}(0)}=\frac{\tilde{w}_{\Gamma X}+w_c}{w_{ph}}; \tag{4.8}$$

the logarithmic derivative of I_{ph} at $t=0$,

$$-\left[\frac{1}{I_{ph}}\frac{dI_{ph}}{dt}\right]_{t=0}=\tilde{w}_{\Gamma X}+w_c+\sum_i w_{ph}^i; \tag{4.9}$$

and the logarithmic derivative of I_{ph} at long times ($t\geqslant 15$ μs),

$$-\lim_{t\to\infty}\left[\frac{1}{I_{ph}}\frac{dI_{ph}}{dt}\right]=w_c+\sum_i w_{ph}^i. \tag{4.10}$$

Since $\Sigma_i w_{ph}^i$ is much smaller than both $\tilde{w}_{\Gamma X}$ and w_c, we can safely neglect $\Sigma_i w_{ph}^i$ in Eqs. (4.9) and (4.10). The decay of $I_{ph}(t)$ is reasonably fitted by

$$I_{ph}(t)=I_0\frac{\exp\left[-\left(w_c+\sum_i w_{ph}^i\right)t\right]}{(1+\alpha^{-1}\tilde{w}_{\Gamma X}t)^\alpha}\simeq I_0\frac{\exp(-w_c t)}{(1+\alpha^{-1}\tilde{w}_{\Gamma X}t)^\alpha}, \tag{4.11}$$

with $0.45<\alpha<1$ depending on the position on the sample. The corresponding distribution function $p(w_{\Gamma X})$ is

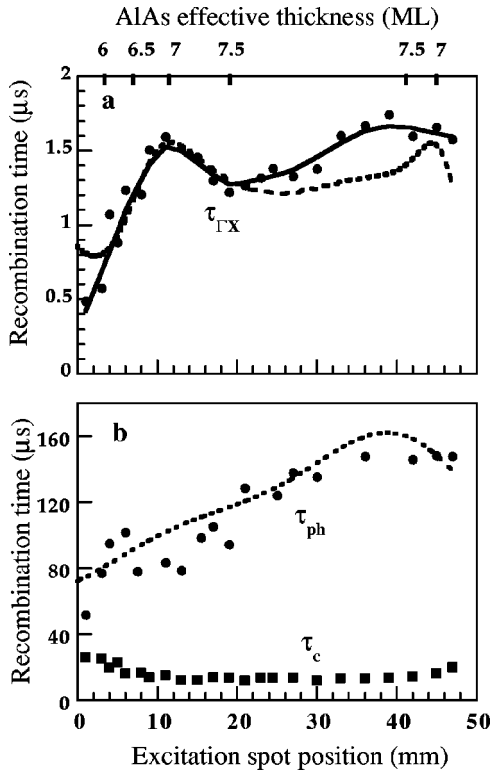

FIG. 9. Sample A1: (a) experimental radiative time due to the Γ-X coupling $\tau_{\Gamma X}$ [experimental, circles (the thick solid line is a guide for the eyes); calculated, dotted line]; (b) recombination time for phonon-assisted transition τ_{ph} (experimental, circles; calculated, dotted line) and inverse of the cutoff frequency τ_c (squares).

$$p(w_{\Gamma X})=0 \quad \text{for} \quad w_{\Gamma X}\leqslant w_c,$$

$$p(w_{\Gamma X})=\left[\frac{\alpha}{\tilde{w}_{\Gamma X}}\right]^{\alpha}\frac{(w_{\Gamma X}-w_c)^{\alpha-1}}{\Gamma(\alpha)} \times\exp\left[-\frac{\alpha(w_{\Gamma X}-w_c)}{\tilde{w}_{\Gamma X}}\right] \quad \text{for} \quad w_{\Gamma X}>w_c, \tag{4.12}$$

where Γ stands for the gamma function. The analytical expression of $p(w_{\Gamma X})$ is close to the one used to describe the Γ-X coupling due to alloy fluctuations in bulk III-V alloys.[38]

The decay times $\tau_c=(w_c)^{-1}$, $\tau_{ph}=(w_{ph})^{-1}$, and $\tau_{\Gamma X}=(\tilde{w}_{\Gamma X})^{-1}$ are shown in Fig. 9. τ_c, of the order of 15 μs, is almost constant over sample A1. Our interpretation of the physical origin of τ_c is as follows. The ZPH radiative recombination rate of excitons depends on the AlAs effective thickness at the localization site. For a fraction of the exciton population this recombination rate is very small. We assume that during their long lifetime these excitons have the opportunity to migrate to other localization sites where the radiative recombination rate due to the Γ-X coupling is larger. Spectral and spatial diffusion of excitons can be described as tunneling assisted by acoustical phonons. The associated tunneling frequency depends on the energy difference and distance between sites. w_c is interpreted as the average tunneling frequency. It can be easily shown that the long-time behavior of PL is governed by the tunneling time if there is a distribution of the radiative recombination rates and if the tunneling rate is much smaller than the average radiative rate.

The experimental values of τ_{ph} are shown by circles in Fig. 9(b). The dotted line represents the calculated quantity $f_{ph}|E_\Gamma-E_X+h\nu_{ph}|^2/|\langle\psi_\Gamma|\psi_X\rangle\langle\psi_\Gamma|\psi_{HH_1}\rangle|^2$ where the prefactor f_{ph} was taken to be 5.1×10^{-4} μs meV^{-2} in order to reproduce the experimental data. The increase of τ_{ph} across the sample is mainly due to the increase of $(E_\Gamma-E_X)$. Here f_{ph} can be expressed as $T_0/M^2_{\text{el-ph}}$ where T_0 is related to the radiative time τ_0 of the direct Γ-HH_1 excitonic transition by $T_0=\tau_0|\langle\psi_\Gamma|\psi_{HH_1}\rangle|^2$. Taking T_0 between 0.5 ns and 1 ns, we find $M_{\text{el-ph}}$ in the range 1–1.4 meV. This value is in good agreement with those determined for SL's.[30]

$\tau_{\Gamma X}$ is shown in Fig. 9(a). It varies between 0.5 and 1.7 μs. It should be noted that this radiative time does not exactly describe the decay of the whole population of localized excitons but only of those whose radiative rate $w_{\Gamma X}$ is larger than the escape frequency w_c. In agreement with the time-integrated data we observe a maximum of $\tau_{\Gamma X}$ around the position 10 mm and possibly around 40 mm, where the ratio I_{zph}/I_{ph} shows minima. In the next section we develop a model describing the Γ-X coupling for localized excitons. This model accounts well for the amplitude of variation of $\tau_{\Gamma X}$.

V. MODEL

A. Γ-X coupling in the case of an interface alloy monolayer

The generalized envelope-function approximation to describe the Γ-X coupling for ideal SL's was developed by Aleiner and Ivchenko[21] and Fu *et al.*[20] In this approach the application of generalized boundary conditions for matching the envelope functions ψ_Γ, ψ_X and their derivatives at interfaces is equivalent to an inclusion of the Γ-X mixing potential $V_{\Gamma X}$ acting on the envelope functions as a sum of δ functions at each interface, namely,

$$V_{\Gamma X}(z)=\sum_i t_{\Gamma X} a V \eta(z_i)\delta(z-z_i). \tag{5.1}$$

Here the interfaces are taken as As planes at positions z_i, $V=\hbar^2/(2m_0a^2)$, a is a parameter with the dimension of length, say, the lattice constant a_0, m_0 is the free-electron mass, $t_{\Gamma X}$ is a dimensionless coupling parameter, and $\eta(z_i)$ is the phase factor of the Bloch X zone-edge wave function: if the origin $z=0$ is taken at one of As planes, it can be presented as

$$\eta(z_i)=\cos\frac{2\pi z_i}{a_0}=(-1)^{2z_i/a_0}. \tag{5.2}$$

It should be mentioned that the full treatment of the Γ-X coupling requires making allowance for a two-subband electron dispersion near the X point and coupling of Γ_1 states with both X_1 and X_3 states.[15,20,21] We use here a simplified model in which the X_3 states are ignored and only the Γ_1-X_1 coupling is considered. In this case the z_i-dependent coupling coefficient

$$t_{\Gamma X}(z_i)=t_{\Gamma X}\eta(z_i) \tag{5.3}$$

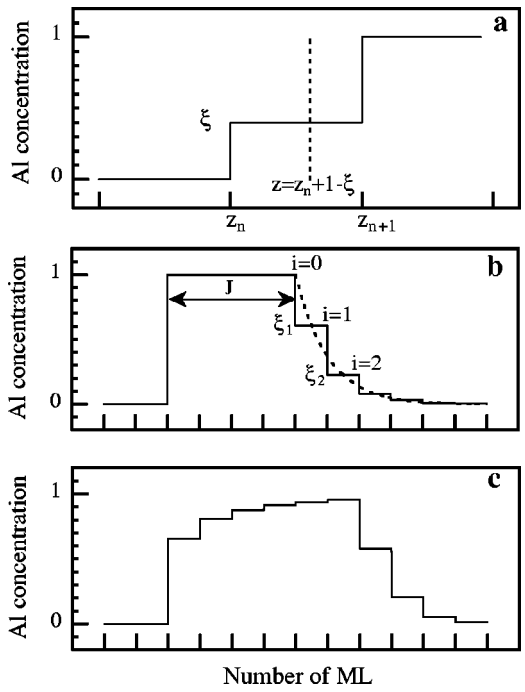

FIG. 10. (a) Schematic representation of a GaAs/AlAs interface region with 1 ML of GaAlAs alloy, (b) Schematic representation of a GaAs/AlAs/GaAs barrier with very asymmetrical interface profiles, the dotted line indicates the exponential decrease of Al concentration, and (c) interface profiles deduced from the segregation model.

in Eq. (5.1) is the same for GaAs/AlAs and AlAs/GaAs interfaces.

In a real GaAs/AlAs structure the interface can hardly be defined as an ideal As plane. Fluctuations of the interface position over 1 or 2 ML's, when averaged over a certain in-plane distance along the layer plane, result in an effective interface position which can be located anywhere between two As planes. Moreover, even in regions with fixed interface position, the segregation process during the sample growth results into a smoothly rising Al concentration from the GaAs to the AlAs layer.[39,40] Hence there is a need to evaluate the Γ-X coupling in the case of fluctuating or nonabrupt interfaces. The idea is to obtain an expression similar to Eq. (5.1) but with a coupling coefficient $t_{\Gamma X}(z_i)$ continuously dependent on z_i. A nonabrupt interface is modeled here by considering 1 ML of $Ga_{1-\xi}Al_{\xi}As$ alloy between pure GaAs and pure AlAs. We define an equivalent abrupt interface at $z_i = z_n + 1 - \xi$ where $z = z_n$ is the position of the As plane after the last pure Ga plane (in units of ML) [Fig. 10(a)]. From $\xi = 1$ to $\xi = 0$ the interface moves from $z_i = z_n$ to $z_i = z_{n+1} = z_n + 1$ and the coefficient $t_{\Gamma X}(z_i)$ in Eq. (5.3) jumps from $+t_{\Gamma X}$ to $-t_{\Gamma X}$, with the arbitrary choice $\eta(z_n) = 1$. For any z_i between z_n and z_{n+1} we define a function $t_{\Gamma X}(z_i)$ which continuously varies between the above limits.

Let us analyze properties of the function $t_{\Gamma X}(z_i)$. Since any Bloch function at the X point changes its sign under the translation by the basic vector $\boldsymbol{\tau} = (a_0/2)(0,1,1)$, i.e., by 1 ML along the axis $z \| [001]$, one can write

$$t_{\Gamma X}(z_i + 1) = -t_{\Gamma X}(z_i) \tag{5.4}$$

for any z_i. In particular, this means that $t_{\Gamma X}(z_i)$ is a periodic function with period $d = 2$ as one can expect from the beginning.

Now we consider a left $Ga_{1-\xi_L}Al_{\xi_L}As$ interface layer between GaAs and AlAs and the next $Ga_{1-\xi_R}Al_{\xi_R}As$ right interface layer, each of them consisting of 1 ML of alloy, and denote the corresponding equivalent abrupt interfaces as z_L and z_R. The Γ-X coupling matrix element is then written

$$\begin{aligned} M_{\Gamma X} &= a_0 V \langle \psi_\Gamma | t_{\Gamma X}(z)[\delta(z - z_L) + \delta(z - z_R)] | \psi_X \rangle \\ &= a_0 V [\psi_\Gamma(z_L)\psi_X(z_L)t_{\Gamma X}(z_L) + \psi_\Gamma(z_R)\psi_X(z_R)t_{\Gamma X}(z_R)]. \end{aligned} \tag{5.5}$$

It is easy to check that the parity rule is verified for interfaces located on As planes ($\xi_R, \xi_L = 0$ or 1). If $\xi_R = \xi_L = \xi$ ($0 < \xi < 1$) and the thickness of pure AlAs is an odd number of ML's, $m = 2p + 1$, then the central plane of the AlAs layer is an Al plane and the coupling is forbidden as well from the same symmetry considerations. The coefficients $t_{\Gamma X}^{L,R}$ for the left and right interfaces must thus verify the additional condition

$$t_{\Gamma X}^{L} + t_{\Gamma X}^{R} = 0,$$

that is,

$$t_{\Gamma X}(z_n + 1 - \xi) + t_{\Gamma X}(z_n + 2p + \xi) = 0$$

or

$$t_{\Gamma X}(-\xi) = t_{\Gamma X}(\xi) \quad (0 \leqslant \xi \leqslant 1). \tag{5.6}$$

The established properties allow one to expand the function $t_{\Gamma X}(z_i)$ in the Fourier series as

$$t_{\Gamma X}(z_i) = t_{\Gamma X} \sum_{p=0}^{\infty} C_p \cos \pi(2p+1) z_i, \tag{5.7}$$

where $\Sigma_p C_p = 1$.

In the following we shall use for $t_{\Gamma X}(z)$ either a triangular function:

$$\begin{aligned} &t_{\Gamma X}(z) = t_{\Gamma X}[1 - 2(z - 2n)] \ \text{ for } \ 2n \leqslant z < (2n+1), \\ &t_{\Gamma X}(z) = t_{\Gamma X}[-1 + 2(z - 2n - 1)] \ \text{ for } \\ &\qquad (2n+1) \leqslant z < (2n+2), \end{aligned} \tag{5.8}$$

or a cosine function $t_{\Gamma X}(z) = t_{\Gamma X} \cos(\pi z)$, in order to simplify the calculations.

B. Extension of the model in the case of gradual interfaces over several ML's

Let us now try to extend this model in the case of a GaAs/AlAs interface region extending over several ML's of GaAlAs alloy with rising concentration in Al. Hereafter, for the sake of simplicity, we shall neglect the variation of the envelope functions across the interface region. The generalized boundary conditions for matching the wave functions ψ_Γ and ψ_X and their derivatives at an A/B interface are expressed as a matrix relation.[15,20,21] In a simplified approach the diagonal matrix coefficients take the value 1 and the off-

diagonal coefficients the values 0 or $t_{\Gamma X}^{AB}$. For an A/B/C structure, provided that the B layer is thin enough, it is easily shown that $t_{\Gamma X}^{AB}$ can be replaced by $t_{\Gamma X}^{AC}=t_{\Gamma X}^{AB}+t_{\Gamma X}^{BC}$, the other coefficients being unchanged. In the previous section we have actually described the case of three layers with concentrations ξ_i: GaAs ($\xi_0=0$), GaAlAs ($\xi_1=\xi$), and AlAs ($\xi_2=1$). Taking a linear variation of $t_{\Gamma X}(z)$ for $0\leqslant z\leqslant 1$, namely, $t_{\Gamma X}(z)=t_{\Gamma X}[1-2z]$, with z defined as $z=1-\xi$, is equivalent to writing a mixing coefficient for the interface region:

$$t_{\Gamma X}^{\text{int}}=t_{\Gamma X}[(\xi_1-\xi_0)-(\xi_2-\xi_1)]. \tag{5.9}$$

This means that the Γ-X mixing coefficient at an As plane is taken proportional to the difference of Al concentrations on either side. For a gradual interface profile we shall generalize this expression and write the coupling coefficient as

$$t_{\Gamma X}^{\text{int}}=t_{\Gamma X}\sum_{i=0}^{\infty}(-1)^i|\xi_{i+1}-\xi_i|. \tag{5.10}$$

Recently the Γ-X coupling was calculated by means of a pseudopotential method for $(\text{GaAs})_M/(\text{AlAs})_M$ SL's in the case of very asymmetrical interface profiles: one of them abrupt and the other one extending over several ML's.[18] It was shown that the coupling is maximum for odd M and minimum and close to zero for even M. Interface graduality and asymmetry not only reduce the coupling but, in this particular case, also lead to an inversion of the parity effect. These results are qualitatively well reproduced within our simple model. Let us consider a DQW GaAs/AlAs/GaAs with an abrupt left GaAs/AlAs interface profile and a gradual right AlAs/GaAs interface profile [Fig. 10(b)]. We take for the right interface an exponential concentration profile similar to that of Ref. 18, $\xi_i=\exp[-(i-\frac{1}{2})/\sigma]$ for $i>1$ and $\xi_0=1$ with σ in units of ML. Using Eq. (5.10) the Γ-X matrix element resulting from the contributions of the left and right interfaces is

$$M_{\Gamma X}\propto t_{\Gamma X}V\left\{1+(-1)^J\frac{\left[1-\exp\left(-\frac{1}{2\sigma}\right)\right]^2}{1+\exp\left(-\frac{1}{\sigma}\right)}\right\}, \tag{5.11}$$

where J is the number of AlAs ML's between the left abrupt interface and the As plane with index $i=0$. Let us choose $\sigma=1$. Then the total quantity of AlAs is an integer number of ML equal to $M=J+\sigma=J+1$. From Eq. (5.11) one obtains $M_{\Gamma X}^{M=2p}\propto 0.89Vt_{\Gamma X}$ and $M_{\Gamma X}^{M=2p+1}\propto 1.11Vt_{\Gamma X}$. The Γ-X coupling potential is larger for odd M than for even M. The parity effect is much attenuated and inverted with respect to the one predicted for abrupt interfaces. For the right interface the largest contribution to the coupling is the first coupling term across the $i=0$ As plane as if the effective AlAs thickness were $J=M-1$. If we choose now $\sigma=2$, the parity effect is the same as for abrupt interfaces although strongly decreased.

The question is whether, in our samples, the observed inversion of the parity-related optical selection rule can be explained by the existence of very asymmetrical interface profiles. Assuming that segregation occurs during the growth, the Al concentration profile can be determined using the models described in the literature. The models assuming thermodynamical equilibrium[39] or the kinetic model[40] are equivalent at the growth temperature used for our samples. We have calculated $M_{\Gamma X}$ with these Al concentration profiles [Fig. 10(c)]. Using Eq. (5.10) we find $M_{\Gamma X}^{M=6}\propto 0.67Vt_{\Gamma X}$ and $M_{\Gamma X}^{M=7}\propto 0.42Vt_{\Gamma X}$. There is no inversion of the parity effect with respect to abrupt interfaces. Therefore the experimentally observed inversion of the parity rule cannot be explained by an asymmetry of the interface profiles.

VI. DISCUSSION

A. Sample A

In Sec. V A we have described the Γ-X coupling in the case of an interface region of width equal to 1 ML. In the following we assume that this model can be applied to a free exciton as well as to a localized exciton since small-scale fluctuations of the interface position are averaged over the relative motion of the electron and the hole. We calculate the Γ-X coupling for a localized exciton as if the exciton were free with the electron located in an AlAs layer of effective thickness e which can be different from an integer number of ML's. Moreover, at each position y along the sample, the PL line is the sum of the contributions of excitons localized in different sites with position $z_L(y)$ of the left interface and $z_R(y)$ of the right interface distributed around their mean values $\overline{z_L}(y)$ and $\overline{z_R}(y)=\overline{z_L}(y)+\overline{e}(y)$. Here $\overline{e}(y)$ is taken as the average AlAs thickness determined by the calibration augmented by 1.1 ML to take into account exciton localization. Let us return to sample A1. What is $\overline{z_L}(y)$? Even with a perfectly flat substrate surface, after the growth of the calibration structure and the $Ga_{0.6}Al_{0.4}As$ alloy layer with thickness gradient, the sample surface is no longer flat but convex. There is a difference of height of about 200 ML from the center to the edge of the wafer. Therefore $\overline{z_L}(y)$ is taken as the y-dependent position of the GaAs/AlAs interface of the DQW calculated by adding the thicknesses of the calibration structure, the alloy layer, and the first GaAs layer of the DQW.

We calculate $M_{\Gamma X}(y)$ using for $t_{\Gamma X}(z)$ the cosine function. Equation (5.5) becomes for each y position

$$M_{\Gamma X}(y)=t_{\Gamma X}a_0V(\psi_\Gamma^L(y)\psi_X^L(y)\cos[\pi z_L(y)]+\psi_\Gamma^R(y)\psi_X^R(y)\cos\{\pi[z_L(y)+e(y)]\}). \tag{6.1}$$

The wave functions ψ_Γ and ψ_X are calculated using equivalent abrupt interfaces and an AlAs thickness equal to e. The quantity $|U_{\Gamma X}|^2=|M_{\Gamma X}|^2/(t_{\Gamma X}a_0V)^2$ is plotted in Fig. 11(a) as a function of position on sample A1 using the values of $\overline{z_L}(y)$ and $\overline{e}(y)$. The small-period and large-period oscillations arise from the variation of $\overline{z_L}(y)$ and $\overline{e}(y)$, respectively. Let us examine three different models that can be used to calculate the average value $|U_{\Gamma X}|_{av}^2$.

(i) Uncorrelated Gaussian fluctuations of z_L and z_R with distribution functions $P_l(z_L)$ and $P_r(z_R)$. In this case we have

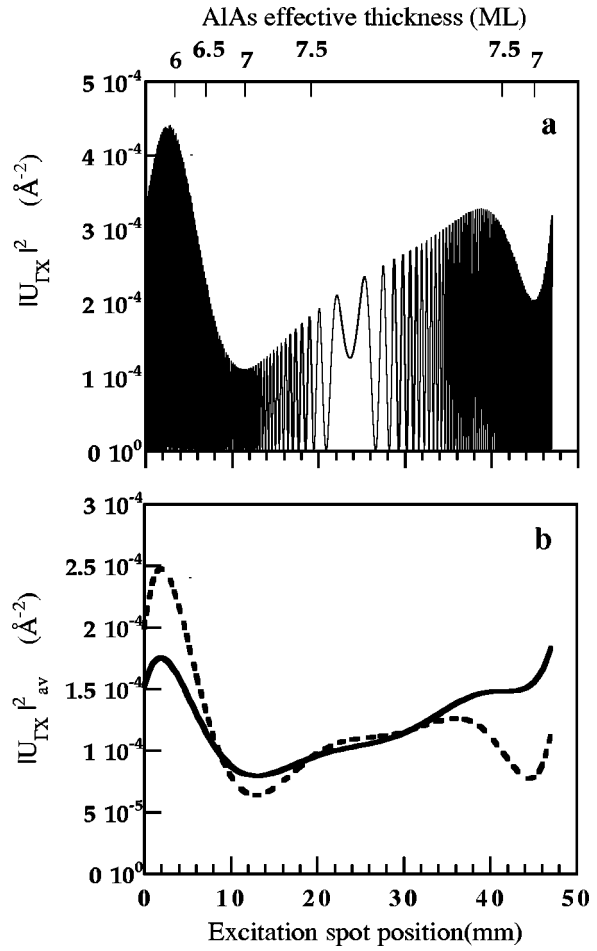

FIG. 11. (a) $|U_{\Gamma X}|^2$ as a function of position along sample A1 (see text) and (b) $|U_{\Gamma X}|^2_{av}$ calculated with model (iii) for the asymmetrical DQW of sample A1 (solid line) for a symmetrical DQW (dotted line).

$$|U_{\Gamma X}|^2_{av} = \int\int dz_L dz_R \times (\psi^L_\Gamma \psi^L_X \cos \pi z_L + \psi^R_\Gamma \psi^R_X \cos \pi z_R)^2 P_l(z_L) P_r(z_R). \tag{6.2}$$

(ii) Correlated Gaussian fluctuations with $z_R(y) = z_L(y) + e(y)$, $e(y) = \bar{e}(y)$. In this case we have

$$|U_{\Gamma X}|^2_{av} = \int dz_L [\psi^L_\Gamma \psi^L_X \cos \pi z_L + \psi^R_\Gamma \psi^R_X \cos \pi (z_L + \bar{e})]^2 P_l(z_L). \tag{6.3}$$

(iii) Uncorrelated Gaussian fluctuations of z_L and e. We have

$$|U_{\Gamma X}|^2_{av} = \int\int dz_L de [\psi^L_\Gamma \psi^L_X \cos \pi z_L + \psi^R_\Gamma \psi^R_X \cos \pi (z_L + e)]^2 P_l(z_L) P_e(e). \tag{6.4}$$

Model (ii) is clearly not adequate. We use for $P_l(z_L)$ a Gaussian function of full width at half maximum $w_l = 1$ ML. The small-period oscillations are well damped but the amplitude variation of $|U_{\Gamma X}|^2_{av}$ remains much too large to fit our experimental results. Model (i) is questionable in the case of very thin AlAs layers where some degree of correlation of interface fluctuations from one interface to the neighboring one is expected.[41] Taking for $P_l(z_L)$ and $P_r(z_L)$ Gaussian profiles of width $w_l = w_r = 1$ ML the small-period oscillations are not sufficiently damped and the amplitude variation of $|U_{\Gamma X}|^2_{av}$ is too small to account for our experimental results. Model (iii) introduces some correlation between the left and right interfaces. This model describes the likely growth process in which large scale monolayer fluctuations at the left interface are reproduced at the right interface whereas additional small scale fluctuations develop at this interface. This model gives the best fit with our experimental results. The distributions $P_l(z_L)$ and $P_e(e)$ in Eq. (6.4) are taken as Gaussian profiles of width $w_l = w_e = 1$ ML. The product $\psi^{L,R}_\Gamma \psi^{L,R}_X$ depends weakly on e. It is taken out of the integral and calculated for $\bar{e}(y)$. Here $|U_{\Gamma X}|^2_{av}$ is plotted in Fig. 11(b). The small-period oscillations are averaged and the overall amplitude of the coupling is reduced. For comparison $|U_{\Gamma X}|^2_{av}$ is also plotted for a symmetrical DQW in Fig. 11(b). The parity effect is of course more pronounced in this case.

We now calculate the radiative decay time

$$\tau^{\rm calc}_{\Gamma X} = g_{\Gamma X} \frac{|E_\Gamma - E_X|^2}{|U_{\Gamma X}|^2_{av} |\langle \psi_\Gamma | \psi_{HH_1} \rangle|^2}, \tag{6.5}$$

where $g_{\Gamma X}$ is a proportionality factor. $\tau^{\rm calc}_{\Gamma X}$ is shown in Fig. 9(a) as a dotted line. The overall behavior and the amplitude of variation of the experimental values of $\tau_{\Gamma X}$ are quite well reproduced. From the fit we obtain $g_{\Gamma X} = 2 \times 10^{-8}$ μs meV^{-2} Å^{-2}. Here $g_{\Gamma X}$ is written as T_0/α^2 with $\alpha = t_{\Gamma X} a_0 V = \hbar^2 t_{\Gamma X}/(2 m_0 a_0)$. We can estimate the strength of the Γ-X coupling potential $V_{\Gamma X} = \alpha \sqrt{|U_{\Gamma X}|^2_{av}}$. The calculated value of $|U_{\Gamma X}|^2_{av}$ is of the order of 1.1×10^{-2} Å^{-2} at the center of the sample. Taking T_0 between 0.5 and 1 ns, α is between 1.58 and 2.23 meV Å and $V_{\Gamma X}$ is found in the range 1.7–2.5 meV. The dimensionless coupling parameter $\tau_{\Gamma X}$ is found in the range 0.23–0.33 in good agreement with other experimental determinations.[36] The value of the coupling parameter is of the right order of magnitude compared to the theoretically calculated one.[15] However, a precise comparison cannot be made since we have not included in our calculation the complexity of the band structure at the zone-edge point, i.e., the X_1-X_3 mixing.

B. Sample B

With the model developed in Sec. V and using the prefactors f_{ph} and $g_{\Gamma X}$ determined for sample A1, we calculate for samples B1 and B2 the quantity

$$\frac{I_{zph}(0)}{I_{ph}(0)} = \frac{\tau_{ph}}{\tau_{\Gamma X}} = \frac{f_{ph}}{g_{\Gamma X}} \left| \frac{E_\Gamma - E_X + \hbar \nu_{ph}}{E_\Gamma - E_X} \right|^2 \frac{|U_{\Gamma X}|^2_{av}}{|\langle \psi_\Gamma | \psi_X \rangle|^2}. \tag{6.6}$$

The variation with the position on the samples is plotted in Fig. 7(c). At the center of the wafer $|U_{\Gamma X}|^2_{av}$ is about 5 times larger than for sample A1 owing to the larger products

$\psi_\Gamma^{L,R}\psi_X^{L,R}$ of the amplitudes of the wave functions at interfaces. Strictly speaking we have to take into account the Γ-X coupling not only at the GaAs/AlAs and AlAs/GaAs interfaces but also at the interfaces between the cladding alloy and the DQW since the ψ_X envelope function extends also in the alloy layers. The amplitude of ψ_X at the alloy/GaAs interfaces is about 5–15 % of the amplitude at the center of the AlAs layer. Nevertheless, the value of $|U_{\Gamma X}|^2_{av}$ across the sample is very close to the one calculated without the coupling at the alloy/GaAs interfaces.

The variation of $\tau_{ph}/\tau_{\Gamma X}$ across the sample reflects mostly the variation of $|U_{\Gamma X}|^2_{av}/|\langle\psi_\Gamma|\psi_X\rangle|^2$ and is dominated by the variation of the oscillating term $\cos[\pi(z_L+e)]$. We have measured the ratio I_{zph}/I_{ph} of the time-integrated PL intensities [Fig. 7(a)]. From the analysis of the PL decay in sample A1, we know that the variation of I_{zph}/I_{ph} is close to the variation of $I_{zph}(0)/I_{ph}(0)$. Therefore the calculated ratio $I_{zph}(0)/I_{ph}(0)=\tau_{ph}/\tau_{\Gamma X}$ can be compared to the experimental ratio I_{zph}/I_{ph}. For sample B1, from the center to the edge of the wafer, the ratio $\tau_{ph}/\tau_{\Gamma X}$ varies by a factor of 2 similarly to the experimental one. For sample B2 the overall behavior of the calculated ratio $\tau_{ph}/\tau_{\Gamma X}$ is in good agreement with the experimental curve although the variation of $\tau_{ph}/\tau_{\Gamma X}$ in the region around 15 mm is not identical to the experimental behavior of I_{zph}/I_{ph}. As mentioned above in Sec. II B the AlAs gradient in the DQW may be slightly different from the one determined from the calibration structure. This may explain the discrepancy.

For both B1 and B2 samples the experimental variation of the ratio I_{zph}/I_{ph} by a factor 2–3 from the center to the edge of the wafer cannot be explained in the frame of a simple model where the matrix element of the Γ-X coupling would depend on the AlAs thickness only through the overlap of the Γ and X envelope functions. On the contrary the amplitude of variation of I_{zph}/I_{ph} across the sample is in good agreement with the ratio $\tau_{ph}/\tau_{\Gamma X}$ calculated with a model taking into account the ML dependence of the Γ-X coupling and the exciton localization. Unfortunately the AlAs gradient, smaller than 1 ML over the wafer, is too weak to give the possibility to observe the oscillations of the coupling matrix element. As mentioned in Sec. IV B 1, contrary to sample A1, the localization of excitons in sites where the AlAs thickness is larger than the average thickness determined from calibration is not necessary to explain the variation of I_{zph}/I_{ph}. This is well in agreement with the observed line splittings in the PL spectrum. They indicate that exciton localization is governed by the hole localization and not by the electron localization.

VII. CONCLUSION

The aim of this work was to demonstrate experimentally the predicted oscillatory behavior of the Γ-X coupling with AlAs layer thickness in GaAs/AlAs type-II heterostructures. We have chosen to study GaAs/AlAs/GaAs DQW structures with thickness gradient. We have shown that the ML dependence of the Γ-X coupling must be observable for GaAs and AlAs thicknesses in the range 2–8 ML.

We have studied the ratio of PL intensities of the ZPH line and the LO phonon replica as well as the time decay of these lines. We have obtained the average radiative recombination time due to the Γ-X coupling, $\tau_{\Gamma X}$, and the recombination time due to phonon-assisted transition, τ_{ph}, as a function of AlAs thickness. For the four samples studied the variation of the Γ-X coupling with AlAs thickness cannot be explained simply by the variation of the overlap of Γ and X_z envelope functions. It clearly shows the ML dependence of the Γ-X mixing potential and its oscillatory behavior with AlAs thickness. For samples B1 and B2 whose PL spectra show ML line splittings, the variation of the ratio of PL intensities of the ZPH line and the LO phonon replica is consistent with the variation of the average AlAs thickness determined by the calibration. For samples A1 and C1 whose PL spectra show a continuous energy shift with layer thicknesses, the variation of the ratio of PL intensities of the ZPH line and the LO phonon replica is consistent with the variation of the average AlAs thickness augmented by $\sim$1 ML to take into account exciton localization. For sample A1 $\tau_{\Gamma X}$ increases by 50% in a region with an average AlAs thickness equal to 6 ML whereas the phonon-assisted recombination time does not show the same variation. We have developed a model describing the Γ-X coupling for excitons localized in regions with fluctuations of the position of interfaces. The exciton is treated as a free exciton in a region with an effective AlAs thickness and nonabrupt interfaces. The amplitude of variation of the experimental radiative time $\tau_{\Gamma X}$ is well reproduced within this model. We obtain an estimation of the Γ-X mixing coefficient $t_{\Gamma X}$.

ACKNOWLEDGMENTS

We are indebted to V. Thierry-Mieg from L2M-Bagneux for the growth of samples and to G. Leroux from CNET-Bagneux for x-ray diffraction.

*Deceased.

[1] G. W. Smith, M. S. Skolnick, A. D. Pitt, I. L. Spain, C. R. Whitehouse, and D. C. Herbert, J. Vac. Sci. Technol. B **7**, 306 (1986).

[2] E. Finkman, M. D. Sturge, M. H. Meynadier, R. E. Nahory, M. C. Tamargo, D. M. Hwang, and C. C. Chang, J. Lumin. **39**, 57 (1987).

[3] K. J. Moore, P. Dawson, and C. T. Foxon, Phys. Rev. B **38**, 3368 (1988).

[4] D. Scalbert, J. Cernogora, C. Benoit à la Guillaume, M. Maaref, F. F. Charfi, and R. Planel, Solid State Commun. **70**, 945 (1989).

[5] H. W. van Kesteren, E. C. Cosman, P. Dawson, K. J. Moore, and C. T. Foxon, Phys. Rev. B **39**, 13 426 (1989).

[6] P. Lefebvre, B. Gil, H. Mathieu, and R. Planel, Phys. Rev. B **40**, 7802 (1989).

[7] Weikun Ge, W. D. Schmidt, M. D. Sturge, L. N. Pfeiffer, and K. W. West, J. Lumin. **59**, 163 (1994).

[8] I. V. Mashkov, C. Gourdon, P. Lavallard, and D. Yu. Roditchev, Phys. Rev. B **55**, 13 761 (1997).

[9] R. I. Dzhioev, H. M. Gibbs, E. L. Ivchenko, G. Khitrova, V. L. Korenev, M. N. Tkachuk, and B. P. Zakharchenya, Phys. Rev. B **56**, 13 405 (1997).

[10] K. Boujdaria, D. Scalbert, and C. Benoit á la Guillaume, Phys.

Status Solidi B **183**, 309 (1994).
[11] V. V. Krivolapchuk, E. S. Moskalenko, A. L. Zhmodikov, T. S. Cheng, and C. T. Foxon, Solid State Commun. **183**, 49 (1999).
[12] E. L. Ivchenko, A. A. Kiselev, Y. Fu, and M. Willander, Phys. Rev. B **50**, 7747 (1994).
[13] J. J. Finley, R. J. Tessier, M. S. Skolnick, J. W. Cockburn, R. Grey, G. Hill, and M. A. Pate, Phys. Rev. B **54**, 5251 (1996).
[14] L. J. Sham and Yan-Ten Lu, J. Lumin. **44**, 207 (1989).
[15] T. Ando, Phys. Rev. B **47**, 9621 (1993).
[16] I. Morrison, L. D. L. Brown, and M. Jaros, Phys. Rev. B **42**, 11 818 (1990).
[17] Lin-Wang Wang and A. Zunger, Phys. Rev. B **56**, 12 395 (1997).
[18] Lin-Wang Wang, A. Franceschetti, and A. Zunger, Phys. Rev. Lett. **78**, 2819 (1997).
[19] T. Ando and H. Akera, Phys. Rev. B **40**, 11 619 (1989).
[20] Y. Fu, M. Willander, E. L. Ivchenko, and A. A. Kiselev, Phys. Rev. B **47**, 13 498 (1993).
[21] I. L. Aleiner and E. L. Ivchenko, Fiz. Tekh. Poluprovodn. **27**, 594 (1993) [Semiconductors **27**, 330 (1993)].
[22] B. A. Foreman, Phys. Rev. Lett. **81**, 425 (1998).
[23] P. C. Klipstein, in *Proceedings of the 24th International Conference on the Physics of Semiconductors*, edited by M. Heiblum and E. Cohen (World Scientific, Singapore, 1998); (unpublished).
[24] H. Im, P. C. Klipstein, R. Grey, and G. Hill, Phys. Rev. Lett. **83**, 3693 (1999).
[25] J. G. Menchero, B. Koiller, and R. B. Capaz, Phys. Rev. Lett. **83**, 2034 (1999).
[26] D. T. Pierce, J. A. Stroscio, J. Unguris, and R. J. Celotta, Phys. Rev. B **49**, 14 564 (1994).
[27] R. M. Wentzcovitch, M. Cardona, M. L. Cohen, and N. E. Christensen, Solid State Commun. **67**, 927 (1988).
[28] F. Minami, T. Nakayama, and K. Inoue, Jpn. J. Appl. Phys., Suppl. **32-1**, 70 (1993).
[29] M. Nakayama, K. Imazawa, K. Suyama, I. Tanaka, and H. Nishimura, Phys. Rev. B **49**, 13 564 (1994).
[30] M. Maaref, F. F. Charfi, D. Scalbert, C. Benoit à la Guillaume, and R. Planel, Phys. Status Solidi B **170**, 637 (1992).
[31] D. Martins, C. Gourdon, P. Lavallard, and R. Planel, Solid State Commun. **114**, 389 (2000).
[32] We use the following parameters: $m_\Gamma = 0.067$ (0.13), $m_{X_z} = 1.3$ (1.1), $m_{X_{xy}} = 0.23$ (0.19), $m_{hh} = 0.38$ (0.46), and $m_{lh} = 0.095$ (0.15), where m_Γ, m_{X_z}, and $m_{X_{xy}}$ are the electron effective masses, in units of the free electron mass, along the growth direction at the band bottom for the Γ, the X_z and the X_{xy} valleys for GaAs (AlAs), respectively. m_{hh} and m_{lh} are the heavy and light hole effective masses along the growth direction, respectively, for GaAs (AlAs). The conduction band offset between GaAs and AlAs is taken as 67% of the band gap offset.
[33] M. Gurioli, J. Martinez-Pastor, M. Colocci, A. Bosacchi, S. Franchi, and L. C. Andreani, Phys. Rev. B **47**, 15 755 (1993).
[34] B. V. Shanabrook and J. Comas, Surf. Sci. **142**, 504 (1984).
[35] W. R. Tribe, P. C. Klipstein, G. W. Smith, and R. Grey, Phys. Rev. B **54**, 8721 (1996).
[36] V. Voliotis, R. Grousson, P. Lavallard, E. L. Ivchenko, and A. A. Kiselev, Phys. Rev. B **49**, 2576 (1994).
[37] B. A. Wilson, C. E. Bonner, R. C. Spitzer, R. Fischer, P. Dawson, K. J. Moore, C. T. Foxon, and G. W. 't Hooft, Phys. Rev. B **40**, 1825 (1989).
[38] M. V. Klein, M. D. Sturge, and E. Cohen, Phys. Rev. B **25**, 4331 (1982).
[39] J. M. Moison, C. Guille, F. Houzay, F. Barthe, and M. Van Rompay, Phys. Rev. B **40**, 6149 (1989).
[40] O. Dehaese, X. Wallart, and F. Mollot, Appl. Phys. Lett. **66**, 52 (1995).
[41] M. V. Belousov, A. Yu. Chernyshov, I. V. Ignatev, I. E. Kozin, A. V. Kavokin, H. M. Gibbs, and G. Khitrova, J. Nonlinear Opt. Phys. Mater. **7**, 13 (1998).